

strip analysis⁴⁻⁶. Relative to free-stream velocity, we measured body angle, wing span, wing elevation, stroke-plane angle of the wing and angular velocity of the wing. Total aerodynamic power (P_{aero}) was calculated as the sum of induced P_{ind} , profile P_{pro} and parasite P_{par} power, and rate change in potential energy. Inertial power, added mass and rate change in kinetic energy were ignored. For the aerodynamic variables contributing to P_{aero} :

$$P_{\text{ind}} = M_b k w (g + A_v) \quad (2)$$

where M_b is body mass, k is the induced velocity correction factor (assumed to be 1.2), w is induced velocity, g is gravitational acceleration, and A_v is vertical acceleration. In our calculation of w , we defined disc area as the area swept by the wings, not a circle⁶.

$$P_{\text{pro}} = 2 \sum_{i=1}^{25} \left(\frac{1}{2} \rho V_{R,i} S_i C_{D,\text{pro}} \right) \quad (3)$$

where V_R is the resultant velocity of a given wing strip, S is the surface area of a wing strip, and $C_{D,\text{pro}}$ is the profile drag coefficient (assumed to be 0.02)^{4,5}. We assumed no change in average wing chord throughout the wing-beat cycle.

$$P_{\text{par}} = \frac{1}{2} \rho S_b C_{D,\text{par}} V_e^2 \quad (4)$$

where S_b is the projected equivalent flat-plate area of body, calculated incorporating body angle relative to free-stream flow⁴, and $C_{D,\text{par}}$ is the parasite drag coefficient (assumed to be 0.13)^{2,6}.

Bone strain and muscle length

Using surgically implanted strain gauges and sonomicrometry crystals, we obtained *in vivo* measurements of bone strain (ϵ_{DPC}) and pectoralis strain (ϵ_{Pect} ; Fig. 1a). Strains were defined with resting (initial) length as that during perching with the bird motionless. A single-element, 1-mm metal-foil strain gauge was placed perpendicular to the long axis of the humerus on the dorsal surface of the delto-pectoral crest (DPC), the insertion for the pectoralis. We assumed that ϵ_{DPC} is proportional to muscle tension. Two 1-mm sonomicrometry crystals (resolution $\pm 15 \mu\text{m}$) were placed 2.5-mm deep, 15-mm apart into the longest fascicles of the mid-belly, the pars sternobrachialis of the pectoralis. We used indwelling electromyography electrodes to measure the timing of pectoralis activity (Fig. 1a).

Calculating pectoralis work and power

Within each wing beat sampled ($n = 979$ wing beats for cockatiels, $n = 1,067$ for doves), we integrated the curve of ϵ_{DPC} plotted as a function of ϵ_{Pect} . The area of these dimensionless loops was converted into work (J) per wing beat by multiplying ϵ_{Pect} by L_{rest} the resting fascicle length (m) of the pectoralis in the region implanted with sonomicrometry crystals, and by multiplying ϵ_{DPC} by F , a force calibration factor (Fig. 1b). We avoided exclusive reliance on our earlier ‘pull-calibration’ technique^{3,7} because we were unable to obtain consistent calibrations in individuals of both species: pull calibrations yielded an average coefficient of variance for F of $29.0 \pm 14.7\%$ in individual birds. Owing to the superficial application of tensile force, this approach also probably engenders larger bending moments than *in vivo* forces transmitted by the muscle at its attachment site, leading to an underestimate of F . Because of these concerns, F was calculated so that mechanical power in the paired pectoralis was set to equal P_{tot} for the subset of wing beats for which kinematics were analysed at 7 and 9 m s^{-1} ($n = 63$ for cockatiels, $n = 29$ for doves). These speeds were chosen because flight at slower speeds is more likely to violate our assumption of quasi-steady flow¹³, and P_{aero} at faster speeds is more sensitive to assumed values of $C_{D,\text{pro}}$ and $C_{D,\text{par}}$. For each bird, pectoralis power, P_{Pect} , was calculated as total work output at a given speed divided by total time in flight at that speed. This approach yielded more consistent calibrations ($\text{cv} = 10.2 \pm 4.2\%$) for F in individual birds.

To evaluate the sensitivity of our aerodynamic-calibration approach, we varied the values of k , $C_{D,\text{pro}}$ and $C_{D,\text{par}}$ for a low- versus a high-power case. In the low-power case, k was decreased from 1.2 to 1.0, and $C_{D,\text{par}}$ and $C_{D,\text{pro}}$ were decreased by 50% to 0.065 and 0.01, respectively; for the high-power case, k was assumed to be 1.4, and $C_{D,\text{par}}$ and $C_{D,\text{pro}}$ were increased by 50% to 0.195 and 0.03. This allowed us to bracket the likely range of pectoralis power that might be observed at any particular flight speed (Fig. 2a, b). We also computed relative power, work and wing-beat frequency, all independent of F , by dividing the observed values in physical units by their respective within-species means and multiplying the dimensionless results by 100 to obtain percentages (Fig. 3).

Received 29 July; accepted 29 October 2002; doi:10.1038/nature01284.

1. Ellington, C. P. Limitations on animal flight performance. *J. Exp. Biol.* **160**, 71–91 (1990).
2. Rayner, J. M. V. Estimating power curves of flying vertebrates. *J. Exp. Biol.* **202**, 3449–3461 (1999).
3. Dial, K. P., Biewener, A. A., Tobalske, B. W. & Warrick, D. R. Mechanical power output of bird flight. *Nature* **390**, 67–70 (1997).
4. Rayner, J. M. V. A vortex theory of animal flight. Part 2. The forward flight of birds. *J. Fluid Mech.* **91**, 731–763 (1979).
5. Norberg, U. M. *Vertebrate Flight: Mechanics, Physiology, Morphology, Ecology and Evolution* (Springer, Berlin, 1990).
6. Askew, G. N., Marsh, R. L. & Ellington, C. P. The mechanical power output of the flight muscles of blue-breasted quail (*Coturnix coturnix*) during take-off. *J. Exp. Biol.* **204**, 3601–3619 (2001).
7. Biewener, A. A., Corning, W. R. & Tobalske, B. W. *In vivo* muscle force-length behavior during level flight in pigeons (*Columba livia*). *J. Exp. Biol.* **201**, 3293–3307 (1998).
8. Pennycuik, C. J., Klaasen, M., Kvist, A. & Lindström, Å. Wingbeat frequency and the body drag anomaly: wind-tunnel observations on a thrush nightingale (*Luscinia luscinia*) and a teal (*Anas crecca*). *J. Exp. Biol.* **199**, 2757–2765 (1996).
9. Tobalske, B. W. Biomechanics and physiology of gait selection in flying birds. *Physiol. Biochem. Zool.* **73**, 736–750 (2000).

10. Tobalske, B. W. & Dial, K. P. Effects of body size on take-off performance in the Phasianidae (Aves). *J. Exp. Biol.* **203**, 3319–3332 (2000).
11. Rosser, B. W. C. & George, J. C. The avian pectoralis: histochemical characterization and distribution of muscle fiber types. *Can. J. Zool.* **64**, 1174–1185 (1986).
12. Rosser, B. W. C., Wick, M., Waldbillig, D. M. & Bandman, E. Heterogeneity of myosin heavy-chain expression in fast-twitch fiber types of mature avian pectoralis muscle. *Biochem. Cell Biol.* **74**, 715–728 (1996).
13. Dial, K. P. Activity patterns of the wing muscles of the pigeon (*Columba livia*). *J. Exp. Zool.* **262**, 357–373 (1992).
14. Thomas, A. L. R. On the aerodynamics of birds' tails. *Phil. Trans. R. Soc. Lond.* **B 340**, 361–380 (1993).
15. Hedrick, T. L., Tobalske, B. W. & Biewener, A. A. Estimates of circulation and gait change based on a three-dimensional kinematic analysis of flight in cockatiels (*Nymphicus hollandicus*) and ringed turtle-doves (*Streptopelia risoria*). *J. Exp. Biol.* **205**, 1389–1409 (2002).
16. Pennycuik, C. J., Alterstam, T. & Hedenström, A. A new low-turbulence wind tunnel for bird flight experiments at Lund University, Sweden. *J. Exp. Biol.* **200**, 1441–1449 (1997).

Acknowledgements We thank G. Lauder and F. Jenkins Jr for comments on this work, and the Concord Field Station staff for animal care and help with experiments. This work was supported by grants from the National Science Foundation to A.A.B. and K.P.D., and from Murdock to B.W.T.

Competing interests statement The authors declare that they have no competing financial interests.

Correspondence and requests for materials should be addressed to B.W.T. (e-mail: tobalske@up.edu).

Neuronal synchrony does not correlate with motion coherence in cortical area MT

Alexander Thiele*† & Gene Stoner*

* Salk Institute for Biological Studies, La Jolla, California 92037, USA

Natural visual scenes are cluttered with multiple objects whose individual features must somehow be selectively linked (or ‘bound’) if perception is to coincide with reality. Recent neurophysiological evidence^{1,2} supports a ‘binding-by-synchrony’ hypothesis³: neurons excited by features of the same object fire synchronously, while neurons excited by features of different objects do not. Moving plaid patterns offer a straightforward means to test this idea. By appropriate manipulations of apparent transparency, the component gratings of a plaid pattern can be seen as parts of a single coherently moving surface or as two non-coherently moving surfaces. We examined directional tuning and synchrony of area-MT neurons in awake, fixating primates in response to perceptually coherent and non-coherent plaid patterns. Here we show that directional tuning correlated highly with perceptual coherence, which is consistent with an earlier study⁴. Although we found stimulus-dependent synchrony, coherent plaids elicited significantly less synchrony than did non-coherent plaids. Our data therefore do not support the binding-by-synchrony hypothesis as applied to this class of motion stimuli in area MT.

To confirm that monkeys’ perception is influenced by transparency manipulations⁵⁻⁸, we trained one monkey to distinguish coherent from non-coherent motion. After training, perceptual reports were obtained for nine probe plaids. For eight of these plaids, we manipulated transparency by holding the intensities of the two gratings (thin bar phase) constant and identical, and varying the intensity of the grating intersections⁵⁻⁸. The ninth probe plaid had one bright and one dark grating. We termed this

† Present address: Henry Wellcome Building for Neuroecology, University of Newcastle upon Tyne, NE2 4HH, UK.

plaid ‘depth-ordered non-coherent’ because the bright bars appeared to transparently occlude the dark bars owing to the intersection luminance.

Monkey coherency judgements (Fig. 1a) matched those of humans⁵. The plaid intersection luminance yielding the highest percentage (97%) of non-coherent motion reports was consistent with transparency. Conversely, the luminance yielding the smallest percentage (31%) of non-coherent motion reports was inconsistent with transparency. For depth-ordered non-coherent plaids, 99% of trials were reported as non-coherent (see Supplementary section 1).

On the basis of our psychophysical results, we selected three plaids to test the binding-by-synchrony (BBS) hypothesis. Coherent plaids (Fig. 1b, right) had an intersection luminance that yielded mostly coherent reports. Our non-coherent plaid (Fig. 1b, left), conversely, had an intersection luminance that consistently resulted in non-coherent reports. We also used depth-ordered non-coherent plaids, which humans and our monkey subject usually saw as non-coherent (Fig. 1b, centre). Thus, we used one perceptually coherent plaid and two types of non-coherent plaids in our neurophysiological studies.

We recorded neuronal activity from pairs of directionally selective neurons in macaque area MT from three fixating monkeys (one of which had previously engaged in the behavioural experiments). Applied to motion coherency, the BBS hypothesis implies that two neurons, one preferring the direction of motion of one grating, the other preferring the direction of motion of the other grating, should synchronize for perceptually coherent but not for non-coherent motion⁹.

The majority of our neuronal pairs did not conform to this prediction. Many neuronal pairs exhibited synchrony that was dependent on the direction of motion of individual gratings (Fig. 2a, left panels) and of plaids (Fig. 2a, right panels). Maximal synchrony was often associated with directions of plaid motion other than those central to the BBS hypothesis (Fig. 2a). Moreover, synchrony seen for the directions relevant to the BBS hypothesis was seldom largest for coherent plaids (for example, see Fig. 2).

Our measure of synchrony was the neuronal correlation coefficient (NCC)¹⁰. The larger the NCC, the greater the proportion of spikes with nearly synchronous timing. Figure 3a shows NCCs cross-plotted for the three pairwise plaid comparisons (143 cell pairs; time period analysed: 200–2,000 ms after stimulus onset). Contrary to the BBS prediction, synchrony elicited by our coherent plaids was statistically indistinguishable from that of non-coherent plaids. Surprisingly, synchrony elicited by depth-ordered non-coherent plaids was significantly greater than that for either non-coherent ($P = 0.012$, repeated measurement (RM) analysis of variance (ANOVA), Tukey’s test) or coherent plaids ($P < 0.001$).

To determine whether firing rate was related to coherency and/or synchrony, we calculated average firing rates on the basis of the same neuronal responses used to calculate NCCs and made the same pairwise comparisons. Firing rates elicited by depth-ordered non-coherent and coherent plaids (for which the pattern direction was around 67.5° away from the preferred direction of each neuron) were significantly greater than those elicited by non-coherent plaids (Fig. 3b). Thus, firing rate discriminated different plaids than did synchrony, and neither measure distinguished coherent from both types of non-coherent plaids. Although both neuronal synchrony and firing rates (obtained from plaid motion that is central for testing the BBS) failed to correlate consistently with perceptual coherence, plaid pattern directional tuning curves (based on all eight directions of plaid motion) correlated well. A single measure, the component pattern index (CPI) captures the degree to which these tuning curves reflected responses to the two individual gratings rather than to the pattern as a whole^{4,11,12}. Positive CPI values imply the encoding of two motions, and negative CPI values suggest a single motion representation. Typically, the larger the CPIs the more bi-lobed is the tuning curve. Figure 3c shows CPIs

calculated for the 225 individual neurons that were members of the neuronal pairs used in our synchrony analysis. Both types of non-coherent plaid elicited CPIs that were significantly greater than for the coherent plaid, whereas no significant difference existed between non-coherent and depth-ordered non-coherent plaids. These results confirm that the directional tuning of area MT neurons is correlated with perceptual coherence⁴.

Recently, a related study came to differing conclusions¹³. They report that cortical neurons in visual areas A18 and PMLS of anaesthetized cats synchronize their responses as a function of perceptual motion coherence but show no coherency-related changes in directional tuning. Although interspecies differences could account for the apparent discrepancy, differences in state of consciousness could also have a role. In monkeys, anaesthesia has been reported to disrupt the ability of directionally selective neurons to integrate motion¹⁴. Furthermore, we examined only synchrony between directionally selective neurons with directional preferences near to the direction of motion of the plaid’s two gratings, whereas ref. 13 did not separately present data from neuronal pairs satisfying that restriction. Because of these profound differences, the two studies cannot be compared directly. To determine whether synchrony related to binding had escaped our analyses, we investigated several variations of the BBS hypothesis. It is possible, for example, that synchrony is expressed differently in different classes of directionally selective neurons. On the basis of responses to coherent plaids, directionally selective neurons have been classified into two types¹¹: ‘component’ neurons respond to the motions of the individual gratings, and ‘pattern’ neurons respond to the motion of the plaid as a whole. Pattern neurons are thought to

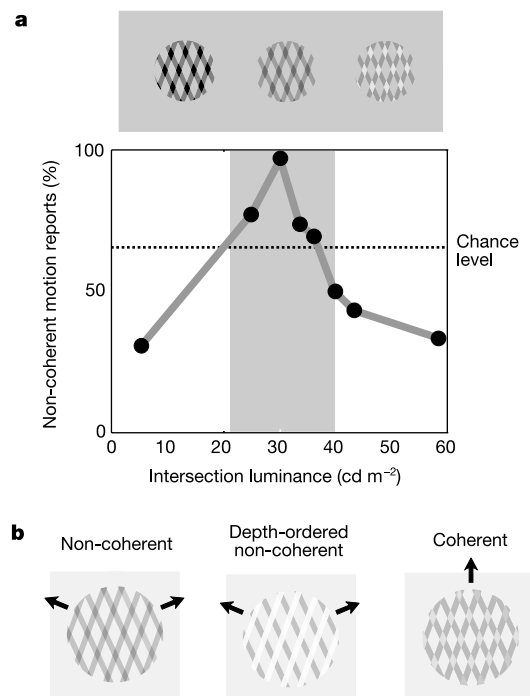


Figure 1 Stimulus and monkey psychophysics. **a**, Monkey perceptual reports as a function of luminance configuration (35 trials per stimulus). The intersection luminance of the probe stimuli (x axis) was varied. Luminance values lying within the central region (grey panel) correspond to stimuli that, when stationary, human subjects usually interpret as one transparent surface overlapping another. When applied to moving plaid patterns, human subjects see maximal non-coherency within this transparency zone²¹. Monkey behavioural data matched that found for humans^{5,21}. Stimulus icons above the graph approximate the appearance of plaids corresponding to the different intersection luminance values. **b**, Three plaids used in neurophysiological experiments. Non-coherent and depth-ordered, non-coherent plaids are seen as two gratings moving independently. Coherent plaids are seen as a single moving object. Arrows indicate perceived motions.

achieve their response properties through component neuron input. Castelo-Branco *et al.*¹³ recorded almost exclusively from component neurons, whereas primate area MT has both component and pattern neurons^{4,11,12}. Rate modulation and synchronization may coexist and complement each other^{9,13} such that synchrony among input neurons determines, in part, the firing rate of recipient higher-order neurons.

On the basis of these assumptions, a scenario consistent with both BBS and the two-stage (component–pattern neuron) model is that component neurons show coherency-related synchrony, whereas pattern neurons show only changes in directional tuning (that is, rate changes for specific directions). If temporal synchrony occurs among component but not pattern neurons, then the pattern neurons in our data set might have masked the synchrony effects of the component neurons. To investigate this possibility, we subdivided neurons into component and pattern types. We analysed separately synchrony between component–component, component–pattern, and pattern–pattern neuronal pairs. For the com-

ponent–component group, depth-ordered non-coherent plaids elicited greater average synchrony than either non-coherent or coherent plaids ($n = 45$, $P < 0.05$, RM-ANOVA, Tukey's test). Although the trend was similar for pattern–pattern and component–pattern neuronal pairs it was not significant, possibly owing to the small sample sizes ($n = 17$, and $n = 28$).

We also examined coherency-related changes in CPI values for pattern and component populations independently. Consistent with previous reports⁴, both neuronal types become significantly ($P < 0.001$) more component-like (their CPI values become larger) when stimulated with perceptually non-coherent plaids compared to coherent plaids. Thus our data do not support a hierarchical binding model in which component neuron synchrony induces changes in the directional tuning of pattern neurons. On the contrary, directional tuning correlates of perceptual coherency are found within both populations of area MT neurons and synchrony consistent with BBS is found in neither.

Another possibility is that BBS occurs in the ON response

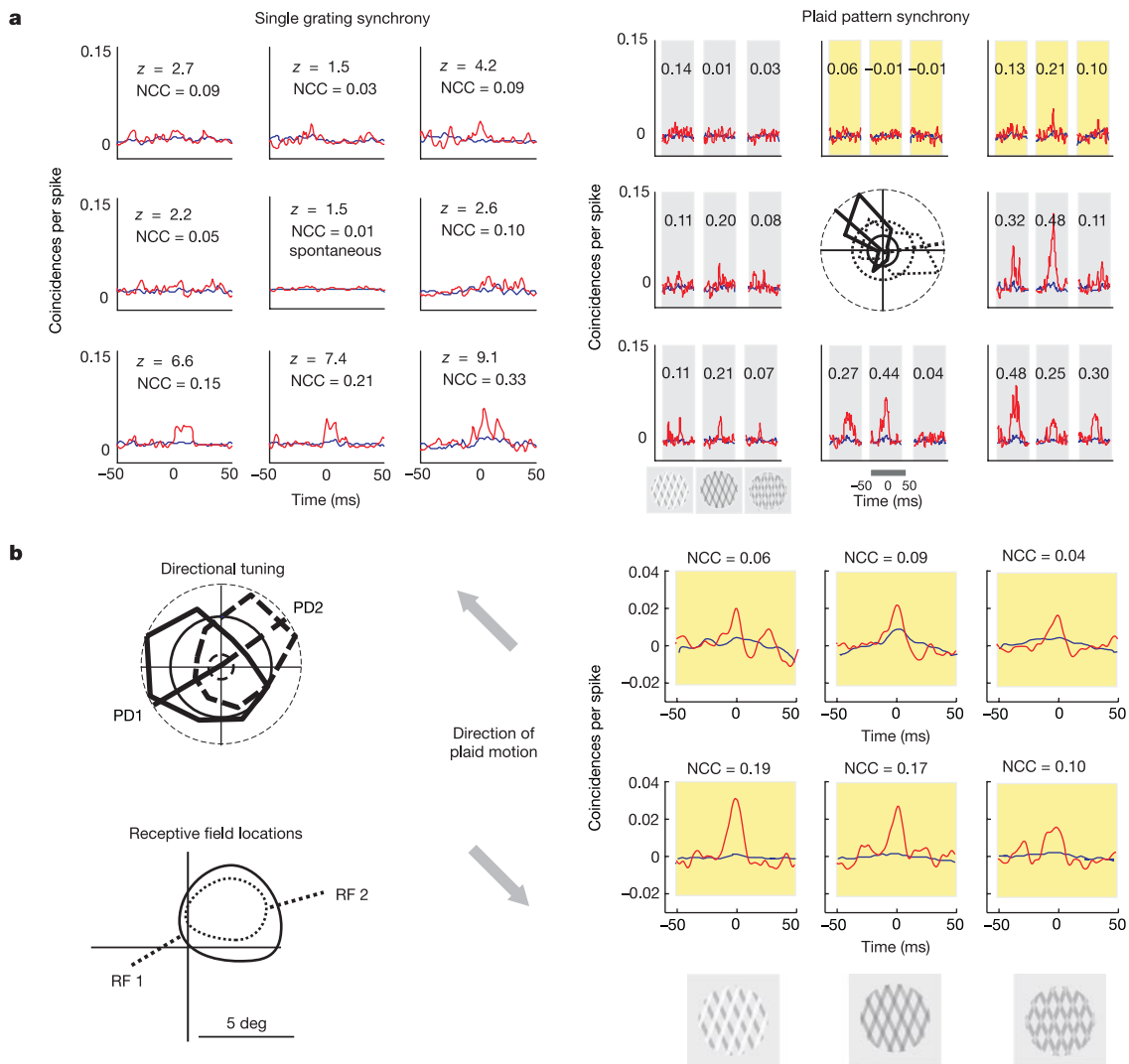


Figure 2 Data from two neuronal pairs. For both pairs, two directions of plaid motion were suitable for testing the binding-by-synchrony (BBS) hypothesis (relevant correlograms are highlighted in yellow). **a**, Responses of a neuronal pair to gratings (left) and plaids (right). Positioning of cross-correlograms (red) and peristimulus time histogram (PSTH) predictors (blue) reflects direction of stimulus motion (left correlogram indicates leftward motion, and so on). Centre inset of right panel shows grating directional tuning curves. Three correlograms in each of the eight subplots of the right panel are for depth-ordered non-coherent, non-coherent, and coherent plaids (from left to right). Neuronal correlation

coefficients (NCCs) are shown above each correlogram. Left panel also shows peak z -scores (z). Synchrony was either greatest for non-coherent plaids or absent altogether. **b**, The second pair showed the least synchrony for coherent plaids. Grating directional tuning curves and receptive fields are shown. For all correlograms, the x axis indicates time interval between spikes from two neuronal recordings and the y axis the number of coincidences. All firing rates are normalized to individual maxima. For tuning curves, dashed and solid lines distinguish individual neurons and vectors indicate the preferred direction of motion (inner dashed and solid circles show spontaneous activity).

transient but that binding is later expressed in firing rates (see ref. 15 for a related finding). To examine this possibility we analysed correlated activity over time periods that included the ON response transient: 30–200 and 30–2,000 ms relative to stimulus onset. The time period of 30–200 ms yielded results qualitatively similar to our initial analysis with depth-ordered non-coherent stimuli eliciting the most synchrony (see Supplementary section 2). However, for this short time period, that difference was only significant when comparing depth-ordered non-coherent and non-coherent stimuli. The time period of 30–2,000 ms yielded results nearly identical to those found for the period after the ON response transient (200–2,000 ms). Thus BBS is found in neither the ON response transient nor the sustained stimulus-response period.

A further possibility is that synchrony serves only to bind features encoded by different hypercolumns⁹. Because the receptive fields of many of our neurons were nearly spatially coincident, both members of some neuronal pairs might be part of the same direction-of-

motion hypercolumn. We divided our neuronal pairs into those with less than 50% receptive field overlap and those with greater than 50% overlap (mean receptive field overlap: $45.4 \pm 48.9\%$, range: 100%; mean receptive field separation: $1.91 \pm 1.71^\circ$, range: 7.61° ; for details see Supplementary section 3). For both sets of neuronal pairs, the depth-ordered stimulus always induced the largest amount of synchrony. However, synchrony differences were slightly greater for cell pairs with non-overlapping receptive fields ($n = 57$, depth-ordered versus coherent: $P = 0.003$; depth-ordered versus non-coherent: $P = 0.037$; coherent versus non-coherent: $P = 0.697$) than for pairs with overlapping receptive fields ($n = 86$, depth-ordered versus coherent: $P = 0.127$; depth-ordered versus non-coherent: $P = 0.021$; coherent versus non-coherent: $P = 0.243$; RM-ANOVA, Tukey's test).

Finally, we examined the contribution of eye movements to neuronal synchrony. Small eye movements (mini-saccades and smooth tracking) unavoidably accompany conscious viewing even during fixation. Tracking eye movements tend to increase perceptual coherence (G.S., unpublished observations) and hence dilute the perceptual differences between stimuli that are intended to be coherent and non-coherent. In addition, eye movements may synchronously activate (or suppress) MT neurons causing stimulus-related changes in neuronal correlation. For these reasons, we analysed data from time periods in which eye movements were absent or minimal. Surprisingly, this analysis revealed that both depth-ordered non-coherent ($P = 0.004$) and non-coherent plaids ($P = 0.01$) elicited significantly more synchrony than did coherent plaids (RM-ANOVA, Tukey's test). For these eye-movement-free periods, no statistical difference in synchrony was found between non-coherent and depth-ordered non-coherent plaids. Thus, during periods of viewing best suited to testing the BBS hypothesis (in which perceptual differences between plaid stimuli are likely to be maximal), we find a result opposite to that predicted by the BBS hypothesis: correlated firing decreases when moving features are perceptually bound into a coherent whole.

Thus we have confirmed that perceptual motion coherency is accompanied by changes in directional tuning within area MT but have found no support for the hypothesis that binding is accompanied by increased neuronal synchrony. Stimulus-induced synchrony was in fact greatest, not for coherent plaids, but for non-coherent plaids. The functional significance, if any, of this synchrony awaits further research. □

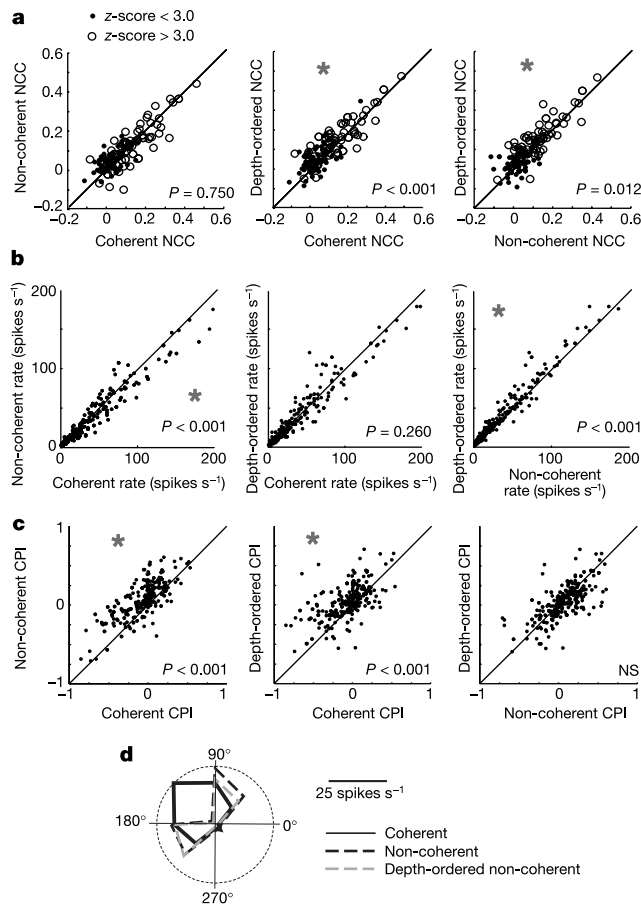


Figure 3 Synchrony magnitude, firing rate and component-pattern indices cross-plotted for each pair-wise stimulus comparison. **a**, Neuronal correlation coefficients (NCCs) were significantly larger for depth-ordered non-coherent than for coherent and non-coherent stimuli. No significant synchrony difference was found between non-coherent and coherent stimuli. Open symbols: z-score synchrony measure exceeded 3.0 for at least one stimulus. Filled symbols: z-score < 3.0 for all stimuli. **b**, Firing rates of individual cells based on the same neuronal responses used to compute synchrony. Rates for depth-ordered non-coherent and coherent plaids were both significantly higher than for non-coherent plaid. **c**, Component pattern index (CPI) values for both non-coherent and depth-ordered non-coherent were significantly greater than for coherent stimuli. **d**, Directional tuning of MT neuron to three plaids. Tuning curves are more component-like for non-coherent and depth-ordered non-coherent plaids than for coherent plaids. For all stimulus comparisons (**a–c**), asterisks indicate significant differences and are positioned on the side of the diagonal with greater magnitude (reflected in the offset of data points).

Methods

General

We recorded from 339 directionally selective cell pairs from area MT in three fixating rhesus monkeys (*Macaca mulatta*). Of these pairs, 143 had directional preferences suitable to testing the BBS hypothesis (sampled from 36, 24 and 23 sites in the three monkeys, respectively). We used a linear four-electrode device (electrode positioning system, Alpha Omega) attached to a custom-built head stage (electrode spacing: 350 μm –800 μm –350 μm). Single units (96 pairs were single units) were isolated using spike-sorting techniques (Alpha Omega). Multi-unit activity (47 pairs) criteria were standard¹⁶ as were the neurophysiological and animal training methods^{15,17}. Experimental protocols conformed to US Department of Agriculture (USDA) regulations and National Institutes of Health (NIH) guidelines for the humane care and use of laboratory animals.

Behavioural task and visual stimuli

Animals fixated a 0.4° diameter target (within ± 1.0 – 1.5°) during 700-ms pre-stimulus and 2,000-ms stimulus presentation period. Stimuli were generated on a cathode ray tube (refresh rate: 60 Hz for a few recordings, 100 Hz otherwise). Plaid stimuli consisted of two superimposed gratings moving at an angle of 135° relative to each other within a circular aperture of 10°. The stimulus was either centred on the fixation spot (97% of the cases) or within 3° of the fixation spot (for extended Methods see Supplementary section 4). In electrophysiological experiments, we used coherent, non-coherent, and depth-ordered non-coherent plaids (for additional details, see Supplementary section 5). Neuronal responses and synchrony were assessed using eight different directions of plaid motion (0–315°, in steps of 45°) and eight directions of single grating motion (corresponding to those in which the plaid components moved; that is 22.5–337.5°, in steps of 45°). Grating duty cycle (thin bar phase grating period) was 0.24. Grating speed was 4° s⁻¹ and the plaid pattern speed was 10° s⁻¹. Neural synchrony was analysed if a cell pair's preferred direction differed by $\geq 90^\circ$ and plaids moved intermediate to the preferred directions of the two cells

(average directional preference difference: $138.3 \pm 26.2^\circ$, range: 89.1°). For cell pairs in which two directions of plaid motion fulfilled these selection criteria, neuronal correlation coefficients (NCCs) were averaged.

Perceptual reports

One monkey reported the direction of moving plaid patterns (six-alternative forced-choice task). During training, the animal viewed plaid patterns with a random-dot texture 'pasted' on the thin bar phase of the gratings (for demonstrations and details see Supplementary section 6). The texture on the two gratings either moved in the same direction (unambiguous coherent motion) or in different directions (unambiguous non-coherent motion). The monkey had one valid choice target for coherent motion and two valid choice targets for non-coherent motion (80% rewards on correct choices). Once performance had reached around 85% correct, we introduced ambiguous probe plaid stimuli on 20% of the trials. On these trials, the monkey was rewarded for reports consistent with either coherent or non-coherent motion.

Data analysis

Baseline firing rates and neuronal synchrony were calculated from 200 ms after fixation onset until stimulus onset (700 ms after fixation onset). Stimulus related activity and synchrony were calculated for three periods: (1) from 200 ms after stimulus onset until 2,000 ms thereafter, avoiding the ON response transient; (2) from the earliest response (30 ms after stimulus onset) until 2,000 ms after stimulus onset; and (3) for the ON response transient only (30–200 ms after stimulus onset). Preferred directions were determined by a vector average method¹⁸ based on direction-of-motion tuning curves in response to gratings. The grating motion direction closest to this vector average was taken as the preferred direction. A neuron was deemed directionally selective if the direction index exceeded 0.5 (direction index = $1 - (\text{anti-preferred activity})/(\text{preferred activity})$; baseline activity subtracted). All cells in this study were directionally selective by this definition.

Cross-correlograms were calculated for each stimulus and prestimulus condition at 1-ms resolution from -50 to $+50$ ms averaged over 10–40 trials. In addition, a peristimulus time histogram (PSTH) predictor was calculated to correct for stimulus-locked synchrony¹⁹. Synchrony was quantified by the NCC¹⁰. We also calculated z-scores^{19,20}, which yielded the same pattern of results as the NCC data (see Supplementary section 7). The NCC was calculated over correlogram time intervals of ± 5 ms, ± 10 ms, ± 20 ms and ± 30 ms relative to time zero. Our overall results were robust with respect to the choice of time intervals. Most pairs had a synchrony peak width of around 10–20 ms centred at time zero. Accordingly, the data plotted in the figures and the corresponding *P*-values were derived from ± 10 -ms time intervals. For an NCC to be included in our data set, the cross-correlograms had to have at least 200 entries. This criterion was usually far exceeded. The CPI was derived from previous work^{11,12} (see Supplementary section 8).

To classify neurons as component- or pattern-like, we computed the average CPI across all three plaid pattern configurations for each neuron. Neurons with large average CPI values (in the upper 50%) of this distribution were classified as component-type whereas neurons with small average CPI values (in the lower 33%) were classified as pattern-type (for justification, see Supplementary section 9) To examine neuronal synchrony unaffected by eye movements, we eliminated periods during and immediately after microsaccades, tracking eye-movements, and eye drifts from our data set. Eye-movement-free periods were subdivided into 200-ms sections and these sections were treated as though they constituted individual trials (see Supplementary section 10).

Received 10 July; accepted 1 November 2002; doi:10.1038/nature01285.

- Gray, C. M., König, P., Engel, A. K. & Singer, W. Oscillatory responses in cat visual cortex exhibit inter-columnar synchronization which reflects global stimulus properties. *Nature* **338**, 334–337 (1989).
- Singer, W. & Gray, C. M. Visual feature integration and the temporal correlation hypothesis. *Annu. Rev. Neurosci.* **18**, 555–586 (1995).
- von der Malsburg, C. & Schneider, W. A neural cocktail party processor. *Biol. Cybern.* **54**, 29–40 (1986).
- Stoner, G. R. & Albright, T. D. Neural correlates of perceptual motion coherence. *Nature* **358**, 412–414 (1992).
- Stoner, G. R., Albright, T. D. & Ramachandran, V. S. Transparency and coherence in human motion perception. *Nature* **344**, 153–155 (1990).
- Stoner, G. R. & Albright, T. D. Motion coherency rules are form-cue invariant. *Vision Res.* **32**, 465–475 (1992).
- Stoner, G. R. & Albright, T. D. Luminance contrast affects motion coherency in plaid patterns by acting as a depth-from-occlusion cue. *Vision Res.* **38**, 387–401 (1998).
- Lindsey, D. T. & Todd, J. T. On the relative contributions of motion energy and transparency to the perception of moving plaids. *Vision Res.* **36**, 207–222 (1996).
- Singer, W. Neuronal synchrony: A versatile code for the definition of relations. *Neuron* **24**, 49–65 (1999).
- Bair, W., Zohary, E. & Newsome, W. T. Correlated firing in macaque visual area MT: time scales and relationship to behavior. *J. Neurosci.* **21**, 1676–1697 (2001).
- Movshon, J. A., Adelson, E. H., Gizzi, M. & Newsome, W. T. *Study Group on Pattern Recognition* (eds Chagas, T., Gattass, R. & Gross, C. G.) 117–151 (Pontificia Academia Scientiarum, Vatican City, 1985).
- Rodman, H. R. & Albright, T. D. Single-unit analysis of pattern-motion-selective properties in the middle temporal visual area. *Exp. Brain Res.* **75**, 53–64 (1989).
- Castelo-Branco, M., Goebel, R., Neuenschwander, S. & Singer, W. Neural synchrony correlates with surface segregation rules. *Nature* **405**, 685–689 (2000).
- Pack, C. C., Berezovskii, V. K. & Born, R. T. Dynamic properties of neurons in cortical area MT in alert and anaesthetized macaque monkeys. *Nature* **414**, 905–908 (2001).
- de Oliveira, S. C., Thiele, A. & Hoffmann, K. P. Synchronization of neuronal activity during stimulus expectation in a direction discrimination task. *J. Neurosci.* **17**, 9248–9260 (1997).

- Kreiter, A. K. & Singer, W. Stimulus-dependent synchronization of neuronal responses in the visual cortex of the awake macaque monkey. *J. Neurosci.* **16**, 2381–2396 (1996).
- Thiele, A., Distler, C. & Hoffmann, K. P. Decision-related activity in the macaque dorsal visual pathway. *Eur. J. Neurosci.* **11**, 2044–2058 (1999).
- Batschelet, E. *Animal Orientation and Navigation* (eds Galler, S. R., Schmidt-Koenig, K., Jacobs, G. J. & Belleville, R. E.) 61–91 (NASA Aeronautics and Space Administration, Washington DC, 1972).
- Aertsen, A. M., Gerstein, G. L., Habib, M. K. & Palm, G. Dynamics of neuronal firing correlation: modulation of "effective connectivity". *J. Neurophysiol.* **61**, 900–917 (1989).
- Eggermont, J. J. & Smith, G. M. Neural connectivity only accounts for a small part of neural correlation in auditory cortex. *Exp. Brain Res.* **110**, 379–391 (1996).
- Stoner, G. R. & Albright, T. D. The interpretation of visual motion: evidence for surface segmentation mechanisms. *Vision Res.* **36**, 1291–1310 (1996).

Supplementary Information accompanies the paper on *Nature's* website (<http://www.nature.com/nature>).

Acknowledgements We thank J. Constanza and D. Diep for technical assistance. We also thank T. D. Albright, J. R. Reynolds, G. Boynton and J. Hegde for discussions on this work and comments on the manuscript.

Competing interests statement The authors declare that they have no competing financial interests.

Correspondence and requests for materials should be addressed to G.S. (e-mail: gene@salk.edu).

Selective gating of visual signals by microstimulation of frontal cortex

Tirin Moore & Katherine M. Armstrong

Department of Psychology, Princeton University, Princeton, New Jersey 08544, USA

Several decades of psychophysical and neurophysiological studies have established that visual signals are enhanced at the locus of attention^{1–5}. What remains a mystery is the mechanism that initiates biases in the strength of visual representations⁶. Recent evidence argues that, during spatial attention, these biases reflect nascent saccadic eye movement commands^{7,8}. We examined the functional interaction of saccade preparation and visual coding by electrically stimulating sites within the frontal eye fields (FEF) and measuring its effect on the activity of neurons in extrastriate visual cortex. Here we show that visual responses in area V4 could be enhanced after brief stimulation of retinotopically corresponding sites within the FEF using currents below that needed to evoke saccades. The magnitude of the enhancement depended on the effectiveness of receptive field stimuli as well as on the presence of competing stimuli outside the receptive field. Stimulation of non-corresponding FEF representations could suppress V4 responses. The results suggest that the gain of visual signals is modified according to the strength of spatially corresponding eye movement commands.

Important stimuli are generally the targets of eye movements, although they can be selectively processed without direct gaze¹. The ability of primates to dissociate the point of gaze from the point of interest does not preclude a common mechanism of attention and eye movement control. Instead, this ability may represent a specialized adaptation that allows covert monitoring, while avoiding the consequences of direct eye contact⁹. For example, it may be adaptive to covertly monitor a surly-looking gentleman seated nearby on a train, whereas confronting him with direct gaze could prove hazardous. Under normal circumstances, shifts in gaze occur freely, and visual detection is facilitated at the location of impending saccades even before the eyes move^{10,11}.